Electron Distribution in a Stable Carbene

Anthony J. Arduengo, III,*,† H. V. Rasika Dias,†,§ David A. Dixon,*,† Richard L. Harlow,*,† W. T. Klooster,*,‡ and T. F. Koetzle‡

Contribution from the DuPont Science and Engineering Laboratory, Experimental Station, Wilmington, Delaware 19880-0328, and Chemistry Department, Brookhaven National Laboratory, Upton, New York 11973-5000

Received November 15, 1993. Revised Manuscript Received May 16, 1994®

Abstract: The synthesis and characterization of the stable carbene perdeuterio-1,3,4,5-tetramethylimidazol-2-ylidene (**2**) are reported. The neutron and X-ray diffraction data from single crystals of this perdeuterocarbene are used to determine the electron distribution in the molecule. Neutron diffraction data were collected at 80 and 173K on **2**. The experimentally determined electron density is very closely matched by density functional calculations which show that **2** is a true carbene with negligible ylidic character.

Introduction

Carbenes essentially represent carbon in oxidation state II. As such, carbenes can be more precisely defined as two-coordinate carbon compounds that have two nonbonding electrons and no *formal charge* on the carbon.[1] Substantial efforts have been made to characterize and understand the electronic nature of carbenes.[2] These highly reactive compounds possess a unique and important chemistry among carbon compounds.[3-6] Detailed experimental structural information on carbenes has not been available due to the transient nature of most carbenes. The synthesis and isolation of a variety of stable carbenes in the imidazol-2-ylidene series has changed this situation.[7-9] Contrary to the usual expectation, the imidazol-2-ylidenes show extraordinary stability and can be easily handled under an inert atmosphere at room temperature.[10] Several X-ray crystallographic studies have been performed on imidazol-2-ylidenes, and precise structural information is now available.[7,8] A number of adducts also have been prepared directly from these stable imidazol-2-ylidenes that provide additional insight into the structure and reactivity of these molecules.[11-20] A preliminary theoretical investigation of the imidazol-2-ylidene system has provided some insight into the unusual stability of these carbenes.[21] A solid-state ^{13}C NMR study of 1,3,4,5-tetramethylimidazol-2-ylidene and its hydrochloride salt recently provided a detailed look at differences in the chemical shielding tensor at a carbene center in comparison with the tensor at a corresponding carbenium center.[22] The comparison of these chemical shielding tensor elements revealed a component (σ_{11}) with a large paramagnetic contribution that is predicted to be characteristic of singlet carbenes.

Earlier work on these imidazol-2-ylidenes has shown that these molecules have structural features which are characteristic of singlet carbenes (*cf.* the small valence angle at carbon, ~102°, and the lengthened bonds to the carbene center).[21,23] The imidazol-2-ylidenes also undergo the structural changes in response to protonation at carbon that are expected for singlet carbenes.[21] Additionally, the wave function at the carbene center

† DuPont Science and Engineering Laboratory.
‡ Brookhaven National Laboratory.
§ Current address: Department of Chemistry, University of Texas at Arlington, Arlington, TX 76019.
∥ Contribution No. 6714.
® Abstract published in *Advance ACS Abstracts*, July 1, 1994.

(1) The term "carbene" was first used in connection with this type of structure in a Chicago taxi; see: Doering, W. v E.; Knox, L. H. *J. Am. Chem. Soc.* **1956**, *78*, 4947, footnote 9. The presence of two nonbonding electrons at carbon is a minimum requirement for an oxidation state II carbon. This is generally possible because a carbon atom has four valence electrons, so if two are involved in bonding, two will remain nonbonding. The restriction to two-coordinate carbon centers excludes one-coordinate carbon structures like vinylidenes, isonitriles, and carbon monoxide, which also can be regarded as oxidation II carbon but obviously have very different bonding possibilities due to the different coordination number and are best considered in a separate category. The requirement that no *formal charge* be present on the carbon is the result of the valence bond structures that are used to depict chemical structures. The general significance of *formal charge* has been previously recognized (Pauling, L. *The Nature of the Chemical Bond*, 3rd ed.; Cornell University Press: Ithaca, 1960; pp 8, 9, and references therein). In the present context this *formal charge* restriction eliminates π-bonded structures like the phenyl anion from consideration (a two-coordinate carbon with a nonbonding pair of electrons but with a *formal negative charge*).
(2) Regitz, M. *Angew. Chem. Int. Ed. Engl.* **1991**, *30*, 674.
(3) Baron, W. J.; Bertoniere, N. R.; DeCamp, M. R.; Griffin, G. W.; Hendrick, M. E.; Jones, M., Jr.; Levin, R. H.; Moss, R. A.; Sohn, M. B. *Carbenes*; Jones, M., Jr., Moss, R. A., Eds.; John Wiley & Sons: New York, 1973; Vol. I.
(4) Closs, G. L.; Gaspar, P. P.; Hammond, G. S.; Hartzler, H. D.; Mackay, C.; Seyferth, D.; Trozzolo, A. M.; Wasserman, E. *Carbenes*; Moss, R. A., Jones, M., Jr., Eds.; John Wiley & Sons: New York, 1975; Vol. II.
(5) Kirmse, W. *Carbene Chemistry*; Academic Press, Inc.: New York, 1971; Vol. 1.
(6) Hine, J. *Divalent Carbon*; The Ronald Press Co.: New York, 1964.
(7) Arduengo, A. J.; Harlow, R. L.; Kline, M. *J. Am. Chem. Soc.* **1991**, *113*, 361.
(8) Arduengo, A. J., III; Dias, H. V. R.; Harlow, R. L.; Kline, M. *J. Am. Chem. Soc.* **1992**, *114*, 5530.
(9) Kuhn, N.; Kratz, T. *Synthesis* **1993**, *1993*, 561.
(10) A very interesting stable phosphaacetylene has been synthesized by G. Bertrand *et al.* This molecule can be regarded as either a phosphaacetylene or a phosphinocarbene. Theoretical models (Dixon, D. A.; Dobbs, K. D.; Arduengo, A. J., III; Bertrand, G. *J. Am. Chem. Soc.* **1991**, *113*, 8782) and a recent X-ray structure on a close analog (Soleilhavoup, M.; Baceiredo, A.; Treutler, O.; Ahlrichs, R.; Nieger, M.; Bertrand, G. *J. Am. Chem. Soc.* **1992**, *114*, 10959) suggest that the phosphaacetylene representation is more appropriate, although the molecule shows some reactivity that is similar to traditional carbenes. See also: (a) Igau, A.; Grutzmacher, H.; Baceiredo, A.; Bertrand, G. *J. Am. Chem. Soc.* **1988**, *110*, 6463. (b) Igau, A.; Baceiredo, A.; Trinquier, G.; Bertrand, G. *Angew. Chem., Int. Ed. Engl.* **1989**, *28*, 621.
(11) Arduengo, A. J., III; Kline, M.; Calabrese, J. C.; Davidson, F. *J. Am. Chem. Soc.* **1991**, *113*, 9704.
(12) Arduengo, A. J., III; Dias, H. V. R.; Calabrese, J. C.; Davidson, F. *J. Am. Chem. Soc.* **1992**, *114*, 9724.
(13) Arduengo, A. J., III; Dias, H. V. R.; Calabrese, J. C.; Davidson, F. *Inorg. Chem.* **1993**, *32*, 1541.
(14) Arduengo, A. J., III; Dias, H. V. R.; Davidson, F.; Harlow, R. L. *J. Organomet. Chem.* **1993**, *462*, 13.
(15) Arduengo, A. J., III; Dias, H. V. R.; Calabrese, J. C.; Davidson, F. *Organometallics* **1993**, *12*, 3405.
(16) Kuhn, N.; Kratz, T.; Henkel, G. *J. Chem. Soc., Chem. Commun.* **1993**, 1778.
(17) Kuhn, N.; Henkel, G.; Kratz, T. *Chem. Ber.* **1993**, *126*, 2047.
(18) Kuhn, N.; Henkel, G.; Kratz, T.; Kreutzberg, J.; Boese, R.; Maulitz, A. H. *Chem. Ber.* **1993**, *126*, 2041.
(19) Arduengo, A. J., III; Gamper, S. F.; Calabrese, J. C.; Davidson, F. *J. Am. Chem. Soc.* **1994**, *116*, 4391.
(20) Arduengo, A. J., III; Tamm, M.; Calabrese, J. C. *J. Am. Chem. Soc.* **1994**, *116*, 3625.
(21) Dixon, D. A.; Arduengo, A. J., III. *J. Phys. Chem.* **1991**, *95*, 4180.
(22) Arduengo, A. J., III; Dixon, D. A.; Kumashiro, K. K.; Lee, C.; Power, W. P.; Zilm, K. W. *J. Am. Chem. Soc.* **1994**, *116*, 6361.
(23) Schaefer, H. F., III. *Science* **1986**, *231*, 1100.

0002-7863/94/1516-6812$04.50/0

of the imidazol-2-ylidenes is very similar to that of singlet carbenes like $:CF_2$.[21] The calculated electron distribution in the imidazol-2-ylidenes does not suggest an overly important role for resonance structures **1b** or **1c** because the dipole moments of the singlet and triplet imidazol-2-ylidene structures are predicted to be similar and the calculated charges at the carbons are small (–0.09*e* for the singlet and 0.07*e* for the triplet).[21] In the experimental structures, the lengthened C–N bonds to the carbene center of the imidazol-2-ylidenes compared to the corresponding carbenium (imidazolium) ions also do not support large contributions from resonance structures **1b** or **1c** to the ground-state structure. These bond length trends are reproduced by theoretical calculations.[21]

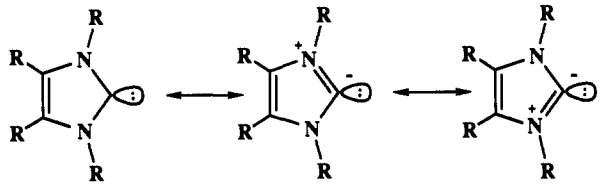

1a **1b** **1c**

Knowledge of the relative contributions of the carbene structure **1a** and the ylidic structures **1b** and **1c** is necessary to decide if it is semantically correct to apply the term "carbene"[1] to such a compound, but far more important is the understanding of how the imidazol-2-ylidenes are stabilized and whether or not they can provide additional information about their more reactive analogs. The structural, theoretical, and reactivity data cited above suggest that structures **1b** and **1c** are not dominant resonance contributors. The question is then Why are the imidazol-2-ylidenes so stable and does resonance play a role in stabilization?

Experimental electron density determination is a technique that can provide considerable insight into chemical bonding.[24,25] To gain additional insight into the bonding of imidazol-2-ylidenes, we have carried out an electron density mapping of the simplest of the carbenes we have isolated thus far, 1,3,4,5-tetramethylimidazol-2-ylidene. This carbene crystallizes in a small unit cell with high symmetry, and the carbene molecule sits on a 2-fold axis so that there are only 11 crystallographically independent atoms in the structure.[8] Carbene molecules are oriented in a head-to-tail fashion along this 2-fold axis so that there are no complicating intermolecular interactions at the carbene center (the closest distance between carbene centers is 600 pm between molecules on adjacent 2-fold axes). Deuterium substitution, which reduces absorption problems for neutron diffraction studies, can be accomplished by modification of the existing synthesis of this carbene. We report here a combination of single-crystal X-ray and neutron diffraction studies to determine the electron distribution in 1,3,4,5-tetramethylimidazol-2-ylidene.

Results and Discussion

Perdeuterio-1,3,4,5-tetramethylimidazol-2-ylidene, **2**, was synthesized as shown in Scheme 1. Deuterated starting materials were either obtained from commercial sources or synthesized as described in the experimental section.

Perdeuterio-1,3,4,5-tetramethylimidazol-2-ylidene has spectroscopic and physical properties very similar to the previously reported protio analog.[8] A single crystal of **2** was grown from a saturated tetrahydrofuran (THF) solution by seeding the solution with a small, well-formed single crystal. The seeded solution was kept at room temperature in a 10-mm NMR tube within a drybox with a nitrogen atmosphere. The THF was allowed to diffuse from the tube through a layer of Parafilm paraffin film covering the top of the tube. After 2 weeks this process produced a single crystal that was approximately 7 mm square by 5 mm thick with a rounded side from the bottom of the NMR tube.

Scheme 1

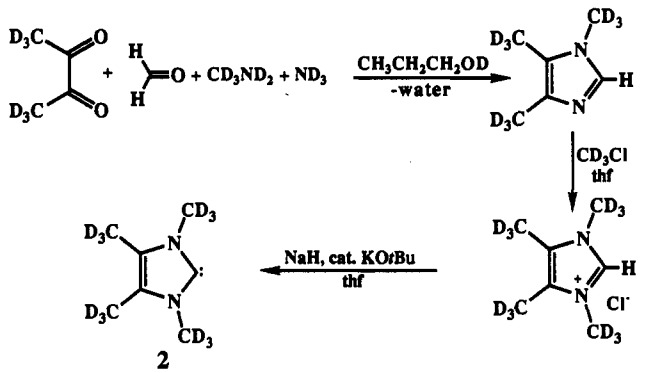

Table 1. Crystal Structure Information for the X-ray and Neutron Diffraction Experiments on **2**[a]

property	X-ray 173 K	neutron 173 K	neutron 80 K
a, pm	977.0(4)	977.7(2)	974.6(2)
b, pm	691.1(3)	692.0(1)	689.9(2)
c, pm	1050.2(5)	1052.6(3)	1042.1(3)
β, deg	94.36(4)	94.28(2)	94.83(3)
V, Å^3	707.0	710.2	698.2
μ, cm^{-1}	0.67	0.013	0.013
reflections collected	3246	1712	1688
unique reflections	833 ($I > 3\sigma(I)$)	897 (all)	877 (all)
parameters	96	103	103
R^{*b}	0.041	0.035	0.030
R_w^{*b}	0.044	0.053	0.061

[a] Monoclinic with space group $C2/c$ and $Z = 4$. [b] For the X-ray study, $R(F_o) = \sum(||F_o| - |F_c||)/\sum|F_o|$; $Rw(F_o) = \sum w(|F_o| - |F_c|)^2/\sum w|F_o|^2$; for the neutron studies, $R(F_o^2) = \sum\Delta/\sum F_o^2$; $wR(F_o^2) = [\sum w\Delta^2/\sum(wF_o^2)^2]^{1/2}$.

The structure of **2** was determined by single-crystal neutron diffraction experiments at 80 K and 173 K and by a single-crystal X-ray diffraction experiment at 173 K. The results of these structure determinations are given in Tables 1-4 and the details of the data acquisition and refinements are given in the Experimental Section. The unit cell parameters for **2** (Table 1) were similar to those previously reported for the protio analog except that the *c*-axis was shorter by about 10 pm.[8] The *R*-factors (Table 1) were low for all three structure determinations, indicating good models of the diffraction data. The fractional cell coordinates (Table 2) of the atoms were similar in the three structure determinations and similar to those found previously for the protio analog.[8] The bond distances and angles from these new structure determinations are given in Table 3 and reflect the characteristic structural features of a singlet carbene (*vide supra*) as found for the protio analog.[8] There were no extraordinary anisotropic thermal parameters (Table 4) for any of the atoms in the three structures, consistent with good matches between the models and data. During the refinement of the model for the X-ray data the deuteriums were allowed to vary with anisotropic thermal parameters, and even these atoms refined smoothly. The final refined structures with thermal ellipsoids are depicted by the ORTEP drawings in Figure 1.

The electron distribution in carbene **2** was calculated from the X-ray and neutron diffraction data obtained at 173 K. Charge deformation terms were introduced on rigid neutral Hartree–Fock pseudoatoms, as described in the Experimental Section. The result of least-squares refinement of the multipole expansion is given in Table 5 along with the form of the expansion. The imidazole ring atoms were expected to have their largest contribution from quadrupole and octapole terms which are required to model the electron distribution associated with a tricoordinated atom involved in π bonding. Interestingly, the

(24) Coppens, P.; Feil, D. In *Applications of Charge Density Research to Chemistry and Drug Design*; Jeffrey, G. A., Piniella, J. F., Eds.; Plenum: New York, 1991; p 7.

(25) Coppens, P. Experimental Electron Density. In *Annual Review of Physical Chemsitry*; Strauss, H. L., Babcock, G. T., Leone, S. R., Eds.; Annual Reviews Inc.: Palo Alto, 1992; p 663.

Table 2. Fractional Coordinates and Equivalent Isotropic Thermal Parameters for Structure Determinations on **2**[a,b]

atom	X	Y	Z	B_{equ}
C_2	0.0000	0.6470(3)	0.2500	2.34
	0.0000	0.6457(2)	0.2500	2.22
	0.0000	0.6483(2)	0.2500	1.06
$N_{1(3)}$	0.0721(1)	0.5218(2)	0.1802(1)	1.98
	0.0724(1)	0.5219(1)	0.1799(1)	2.01
	0.0729(1)	0.5235(1)	0.1798(1)	0.98
$C_{5(4)}$	0.0459(1)	0.3279(2)	0.2050(1)	1.93
	0.0462(1)	0.3283(1)	0.2048(1)	1.89
	0.0465(1)	0.3291(1)	0.2046(1)	0.93
$C_{6(7)}$	0.1689(2)	0.5863(2)	0.0900(2)	2.73
	0.1683(1)	0.5857(1)	0.0903(1)	2.68
	0.1696(1)	0.5871(1)	0.0902(1)	1.28
$C_{9(8)}$	0.1090(2)	0.1663(3)	0.1357(2)	2.78
	0.1087(1)	0.1667(1)	0.1360(1)	2.76
	0.1087(1)	0.1670(1)	0.1349(1)	1.31
$D_{6(7)a}$	0.1766(20)	0.7294(28)	0.0903(19)	5.3
	0.1740(2)	0.7399(2)	0.0950(2)	6.16
	0.1752(1)	0.7434(2)	0.0947(1)	3.16
$D_{6(7)b}$	0.1397(15)	0.5398(26)	0.0045(16)	3.3
	0.1370(1)	0.5403(2)	−0.0054(1)	4.63
	0.1371(1)	0.5423(2)	−0.0076(1)	2.53
$D_{6(7)c}$	0.2602(16)	0.5280(26)	0.1144(14)	3.3
	0.2694(1)	0.5272(2)	0.1147(1)	4.77
	0.2717(1)	0.5275(2)	0.1162(1)	2.60
$D_{9(8)a}$	0.2093(19)	0.1702(25)	0.1482(15)	3.5
	0.2201(1)	0.1693(2)	0.1492(1)	4.55
	0.2212(1)	0.1702(2)	0.1484(1)	2.47
$D_{9(8)b}$	0.0840(18)	0.1791(25)	0.0418(15)	3.6
	0.0813(1)	0.1749(2)	0.0339(1)	4.70
	0.0800(1)	0.1759(2)	0.0313(1)	2.48
$D_{9(8)c}$	0.0776(17)	0.0447(22)	0.1660(16)	3.5
	0.0734(1)	0.0289(2)	0.1707(1)	4.81
	0.0733(1)	0.0281(2)	0.1698(1)	2.52

[a] The three lines per atom contain information from the X-ray study at 173 K, the neutron study at 173 K, and the neutron study at 80 K, respectively. [b] The standard numbering scheme for an imidazole ring is used. Carbons 6 and 7 and 8 and 9 are the substituent methyl groups on nitrogen and carbon, respectively. Due to crystallographic symmetry N_1, C_5, C_6, and C_9 are related to N_3, C_4, C_7, and C_8, respectively, by the symmetry operation $-x$, y $(1/2) - z$.

carbene center C_2 also has a substantial contribution in d_2 which corresponds to a dipole contribution (p-like) along y (the direction of the in-plane lone pair of electrons at this center). Additional contributions at C_2 from q_1, q_5, o_1, o_2, o_3, and o_6 define the electron density associated with the lone pair at the carbene center.

This result is most easily recognized in the diagram of total electron distribution in the molecular plane constructed from the multipole expansion (Figure 2a). Figure 2 includes a drawing of the "valence" electron distribution in the plane that was constructed by omitting the core density at nitrogen and carbon (Figure 2b). The depiction of valence electron distribution thus is not obscured by the high electron density near the nuclear positions and provides a more informative view of the bonding in the molecule. For comparison, a drawing of the in-plane total electron density predicted by a density functional (DFT) calculation on **2** at the geometry observed in the 173 K neutron diffraction structure (*vide infra*) has been included in Figure 2 (Figure 2c). The DFT calculations were done including self-consistent gradient (nonlocal) corrections for exchange[26-28] and correlation.[29] A model for the valence electron density was calculated by the DFT technique using pseudopotentials[30,31] for carbons and nitrogens

(26) Becke, A. D. *Phys. Rev. A* **1988**, *38*, 3098.
(27) Becke, A. D. *The Challenge of d and f Electrons: Theory and Computation*; ACS Symposium Series #394; American Chemical Society: Washington, DC, 1989.
(28) Becke, A. D. *Int. J. Quantum Chem., Quantum Chem. Symp.* **1989**, *23*, 599.
(29) Perdew, J. P. *Phys. Rev. B* **1986**, *33*, 8822.
(30) Chen, H.; Kraskowski, M.; Fitzgerald, G. *J. Chem. Phys.* **1993**, *98*, 8710.
(31) Troullier, N.; Martins, J. L. *Phys. Rev. B* **1991**, *43*, 1993.

Table 3. Bond Distances (pm) and Angles (deg) from the Structure Determinations on **2**

property	X-ray 173 K	neutron 173 K	neutron 80 K
$r(N_{1(3)}-C_2)$	136.4(2)	136.3(1)	136.7(1)
$r(N_{1(3)}-C_{5(4)})$	139.2(2)	139.2(1)	139.4(1)
$r(N_{1(3)}-C_{6(7)})$	145.8(2)	144.8(1)	145.0(1)
$r(C_4-C_5)$	135.1(2)	136.1(2)	136.4(2)
$r(C_{4(5)}-C_{8(9)})$	149.2(2)	148.8(1)	149.0(1)
$r(C_{6(7)}-D_{6(7)a})$	99.2(19)	106.9(2)	108.0(1)
$r(C_{6(7)}-D_{6(7)b})$	97.5(16)	107.7(1)	108.7(1)
$r(C_{6(7)}-D_{6(7)c})$	99.4(16)	108.2(1)	108.9(1)
$r(C_{8(9)}-D_{8(9)a})$	97.9(18)	108.6(2)	109.1(1)
$r(C_{8(9)}-D_{8(9)b})$	100.2(16)	108.9(2)	109.3(1)
$r(C_{8(9)}-D_{8(9)c})$	95.7(16)	109.0(2)	109.5(1)
$\theta(N_1-C_2-N_3)$	101.3(2)	102.0(1)	101.9(1)
$\theta(C_2-N_{1(3)}-C_{5(4)})$	113.6(1)	113.2(1)	113.2(1)
$\theta(C_2-N_{1(3)}-C_{6(7)})$	122.8(1)	123.3(1)	123.3(1)
$\theta(C_{5(4)}-N_{1(3)}-C_{6(7)})$	123.6(1)	123.6(1)	123.5(1)
$\theta(N_{1(3)}-C_{5(4)}-C_{4(5)})$	105.8(1)	105.8(1)	105.8(1)
$\theta(N_{1(3)}-C_{5(4)}-C_{9(8)})$	122.7(1)	123.0(1)	122.9(1)
$\theta(C_{4(5)}-C_{5(4)}-C_{9(8)})$	131.4(1)	131.2(1)	131.3(1)
$\theta(N_{1(3)}-C_{6(7)}-D_{6(7)a})$	110.8(9)	108.0(1)	107.9(1)
$\theta(N_{1(3)}-C_{6(7)}-D_{6(7)b})$	109.8(8)	111.6(1)	111.3(1)
$\theta(N_{1(3)}-C_{6(7)}-D_{6(7)c})$	108.8(9)	110.8(1)	110.8(1)
$\theta(C_{4(5)}-C_{8(9)}-D_{8(9)a})$	111(1)	111.7(1)	111.6(1)
$\theta(C_{4(5)}-C_{8(9)}-D_{8(9)b})$	110(1)	111.1(1)	111.0(1)
$\theta(C_{4(5)}-C_{8(9)}-D_{8(9)c})$	110(1)	110.1(1)	110.1(1)
$\theta(D_{6(7)a}-C_{6(7)}-D_{6(7)b})$	110(2)	110.1(1)	109.6(1)
$\theta(D_{6(7)a}-C_{6(7)}-D_{6(7)c})$	110(1)	108.5(1)	108.9(1)
$\theta(D_{6(7)b}-C_{6(7)}-D_{6(7)c})$	107(1)	107.7(1)	108.3(1)
$\theta(D_{8(9)a}-C_{8(9)}-D_{8(9)b})$	107(1)	107.2(1)	107.2(1)
$\theta(D_{8(9)a}-C_{8(9)}-D_{8(9)c})$	109(1)	108.2(1)	108.5(1)
$\theta(D_{8(9)b}-C_{8(9)}-D_{8(9)c})$	110(1)	108.4(1)	108.4(1)

(Figure 2d). The valence electron distribution drawings (Figure 2b,d) clearly show electron density to the right of the carbene carbon in a direction away from all other bonded atoms. This area of nonbonding electron density represents the in-plane carbene lone pair of electrons. Each of the imidazole ring atoms also shows a trigonal distribution of the in-plane electron density in agreement with the approximate sp^2 hybridizations of these centers. The highest electron density is found around the nitrogens, consistent with their high electronegativity relative to carbon and hydrogen (deuterium). A slight asymmetry is present in the drawings of the experimental electron density. This asymmetry is not real but rather an artifact of the grid that was used to map the electron density. The grid points were mapped at 10-pm intervals but were not centered along the crystallographic 2-fold axis that passes through C_2 and bisects the C_4–C_5 bond. In spite of this minor distortion, it can be seen that there is an excellent agreement between the experimentally determined electron distribution and that calculated with the DFT technique. This level of agreement is found for all views of the electron distribution.

Besides the presence of the in-plane lone pair of electrons at the carbene center, another interesting facet of the electron distribution in **2** is the π electron distribution. Figure 3 illustrates the electron distribution in the π system 35 pm above the molecular plane. The experimental valence density is shown in Figure 3a, and the DFT prediction of the valence density is shown in Figure 3b. Again the agreement between experiment and theory is excellent. There is a clear indication of the double bond between C_4 and C_5. By virtue of their higher nuclear charge the nitrogens again show the highest electron density which now represents the $p\pi$ lone pairs of electrons. The π-bonding regions between nitrogen and carbon show less electron density than is found in the C_4–C_5 double bond area, and the density which is present in these regions tends to contour around nitrogen. The out-of-plane electron density in the space around C_2 is primarily positioned above the in-plane lone pair (outside the ring). This out-of-plane electron density at C_2 is a diminution of the high density found at the in-plane lone pair. Indeed, as can be seen from a planar cross section orthogonal to the molecular plane and bisecting the

Table 4. Anisotropic Thermal Parameters in the Form $\exp[-19.739(U_{11}h^2a^{*2} \ldots + 2(U_{12}hka^*b^* \ldots))]$ for Structure Determinations on **2**[a,b]

atom	U_{11}	U_{22}	U_{33}	U_{12}	U_{13}	U_{23}
C_2	0.0324(9)	0.0284(9)	0.0298(8)	0.0000	0.0137(7)	0.0000
	0.0327(5)	0.0224(5)	0.0311(5)	0.0000	0.0143(4)	0.0000
	0.0154(5)	0.0106(5)	0.0153(5)	0.0000	0.0065(4)	0.0000
$N_{1(3)}$	0.0254(5)	0.0263(5)	0.0249(5)	−0.0020(4)	0.0109(4)	−0.0007(4)
	0.0254(3)	0.0262(3)	0.0259(3)	−0.0016(2)	0.0108(5)	−0.0006(2)
	0.0122(3)	0.0128(3)	0.0131(3)	−0.0007(2)	0.0050(2)	−0.0004(3)
$C_{5(4)}$	0.0258(5)	0.0244(6)	0.0234(5)	0.0011(4)	0.0046(4)	−0.0014(5)
	0.0250(3)	0.0240(4)	0.0233(4)	0.0015(3)	0.0062(3)	−0.0017(3)
	0.0117(3)	0.0118(4)	0.0120(4)	0.0010(3)	0.0030(3)	−0.0011(3)
$C_{6(7)}$	0.0348(7)	0.0391(8)	0.0322(7)	−0.0065(7)	0.0172(6)	−0.0004(7)
	0.0339(4)	0.0381(5)	0.0322(5)	−0.0054(3)	0.0175(3)	−0.0016(3)
	0.0154(4)	0.0178(4)	0.0164(4)	−0.0023(3)	0.0075(3)	−0.0007(3)
$C_{9(8)}$	0.0422(9)	0.0309(7)	0.0333(8)	0.0076(7)	0.0081(7)	−0.0062(6)
	0.0425(5)	0.0298(4)	0.0335(5)	0.0076(3)	0.0091(3)	−0.0061(3)
	0.0190(4)	0.0145(4)	0.0169(4)	0.0036(3)	0.0040(3)	−0.0029(3)
$D_{6(7)a}$	0.083(15)	0.043(12)	0.087(14)	−0.021(11)	0.078(12)	−0.012(11)
	0.1038(11)	0.0435(7)	0.0960(11)	−0.0153(6)	0.0690(9)	−0.0003(8)
	0.0515(8)	0.0219(5)	0.0513(7)	−0.0069(5)	0.0318(6)	−0.0007(4)
$D_{6(7)b}$	0.032(10)	0.066(13)	0.030(9)	−0.025(9)	0.006(9)	−0.001(9)
	0.0543(6)	0.0911(9)	0.0323(5)	−0.0132(6)	0.0148(4)	−0.0003(4)
	0.0294(5)	0.0494(7)	0.0180(5)	−0.0066(4)	0.0065(4)	−0.0011(4)
$D_{6(7)c}$	0.023(9)	0.070(14)	0.035(9)	0.003(9)	0.014(8)	0.007(9)
	0.0347(5)	0.0950(9)	0.0535(6)	−0.0025(6)	0.0177(5)	0.0038(6)
	0.0181(5)	0.0506(7)	0.0311(5)	0.0013(4)	0.0075(4)	0.0036(5)
$D_{9(8)a}$	0.043(11)	0.054(12)	0.038(10)	0.015(10)	0.004(9)	−0.011(9)
	0.0468(6)	0.0638(8)	0.0637(8)	0.0182(5)	0.0133(5)	−0.0106(5)
	0.0230(5)	0.0355(6)	0.0361(6)	0.0086(4)	0.0055(4)	−0.0062(4)
$D_{9(8)b}$	0.065(12)	0.047(11)	0.026(10)	0.012(10)	0.002(9)	−0.009(9)
	0.0784(8)	0.0623(8)	0.0383(6)	0.0158(6)	0.0068(6)	−0.0151(5)
	0.0411(6)	0.0340(6)	0.0191(5)	0.0079(4)	0.0030(5)	−0.0069(4)
$D_{9(8)c}$	0.065(12)	0.015(9)	0.055(11)	0.001(10)	0.010(10)	−0.004(9)
	0.0825(9)	0.0340(6)	0.0688(8)	0.0061(5)	0.0226(7)	−0.0062(5)
	0.0420(7)	0.0178(5)	0.0371(6)	0.0020(4)	0.0109(5)	−0.0015(4)

[a] The three lines per atom contain information from the X-ray study at 173 K, the neutron study at 173 K, and the neutron study at 80 K, respectively. [b] The standard numbering scheme for an imidazole ring is used. Carbons 6 and 7 and 8 and 9 are the substituent methyl groups on nitrogen and carbon, respectively. Due to crystallographic symmetry N_1, C_5, C_6, and C_9 are related to N_3, C_4, C_7, and C_8, respectively, by the symmetry operation $-x, y, (1/2) - z$.

N–C–N angle (*vide infra*, Figure 5a), the electron distribution at C_2 falls to a minimum in the π direction from the in-plane lone pair. The exocyclic C–N and C–C bonds are typical single bonds to the methyls without $p\pi$–$p\pi$ bonding and thus can serve as reference points from which the endocyclic bonds can be evaluated. When these exocyclic bonds are compared with their endocyclic counterparts in parts a and b of Figure 3 only the endocyclic C_4–C_5 bond shows obvious $p\pi$–$p\pi$ bonding. A second cross section of the π system 70 pm above the molecular plane is shown in Figure 3, parts c (experimental valence) and d (DFT valence). These latter two drawings have an outermost contour level of 0.65 eÅ^{-3} but an interval of 0.05 between adjacent contours to provide additional data. At this contouring level 70 pm above the plane the out-of-plane experimentally determined electron density at C_2 has just vanished, yet the C_4–C_5 double bond and nitrogen p π lone pairs are still clearly visible.

Perpendicular contour plots of the experimentally determined π and σ electron distribution in the three unique ring bonds are shown in Figure 4. The electron distribution is symmetric in the C_4–C_5 double bond (Figure 4a). The two types of heteroatomic bonds, C_2–$N_{1(3)}$ (Figure 4b) and $C_{4(5)}$–$N_{3(1)}$ (Figure 4c), both show a very polarized distribution of electrons, as would be expected on the basis of the different nuclear charges of carbon and nitrogen. Furthermore, the perpendicular electron density above and below C_2 falls off faster than the perpendicular density above and below $C_{4(5)}$. The two types of exocyclic bonds are shown if Figure 4, parts d and e. The endocyclic C–N bonds appear quite similar to the exocyclic C–N bonds to the methyl substituents, which suggests that π interactions between carbon and nitrogen centers in the ring are not very well developed. On the other hand the endocyclic C–C bond shows a clear π component relative to its exocyclic counterpart.

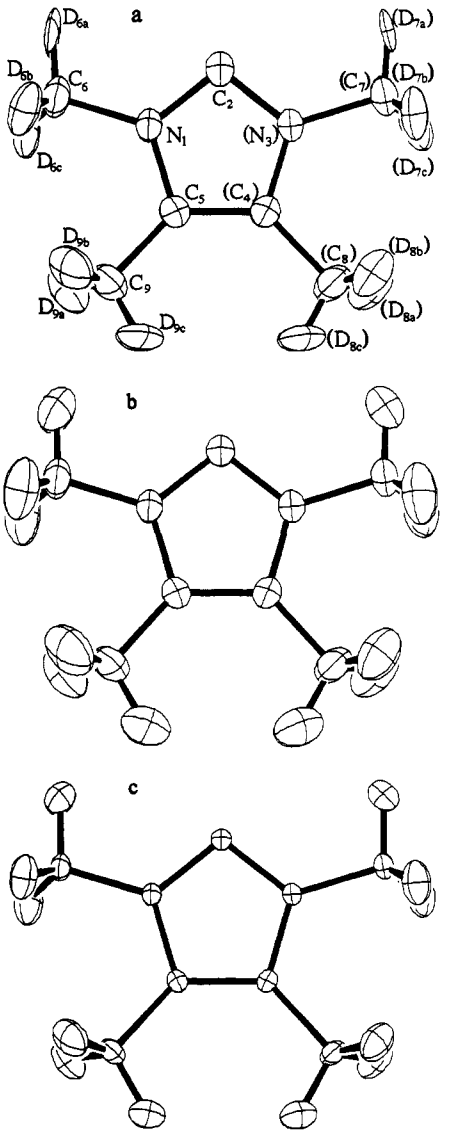

Figure 1. ORTEP drawings (50% probability ellipsoids) of the structures refined for the (a) 173 K X-ray, (b) 173 K neutron, and (c) 80 K neutron diffraction data.

The side view of the carbene center in Figure 5 provides additional insight into the electron distribution around C_2. The plane that has been contoured is orthogonal to the molecular plane and lies along the molecular 2-fold axis. This view allows both the in-plane lone pair and out-of-plane density at the carbene center to be viewed simultaneously. In this orientation it is easy to compare the carbene center in **2** with those in singlet $:CH_2$ and $:CF_2$. The match between the experimental model of electron distribution (Figure 5a) and the theoretical DFT model (Figure 5b) is good. The theoretical DFT models of singlet $:CH_2$ and $:CF_2$ are shown in Figure 5, parts c and d, respectively, for comparison. The distribution of electron density smoothly changes from a high in-plane p character distribution in CH_2 to more spherical distributions in CF_2 and **2**. Nonetheless, a strong in-plane p character contribution is evident even in **2**, and an "egg"-shaped profile is observed.

One final representation of the electron distribution in **2** is the deformation density that is presented in Figure 6. The placement of nonperturbed spherical Hartree–Fock atoms in the atomic positions found in **2** creates a reference "promolecule" from which the deformation density is calculated. This difference plot represents the distortion of experimentally determined electron

Table 5. Electron Population Parameters to Fit the Multipole Expansion[a,b,c]

	P_v	d_1 [x]	d_2 [y]	d_3 [z]	q_1 [x^2-y^2]	q_2 [xy]	q_3 [xz]	q_4 [yz]	q_5 [z^2]	$[x(x^2-3y^2)]$ σ_1	$[y(3x^2-y^2)]$ σ_2	$[z(x^2-y^2)]$ σ_3	α_4 [xyz]	$[x(5z^2-1)]$ σ_5	$[y(5z^2-1)]$ σ_6	$[z(5z^2-3)]$ σ_7
$N_{(1)}$	0.20(5)	−0.58(19)	0.27(20)	0.74(20)	0.07(18)	−0.25(21)	−0.45(19)	0.24(20)	−0.61(19)	1.50(30)	1.90(29)	−1.86(30)	−2.18(31)	0.61(24)	1.44(27)	−0.37(26)
C_2	−0.03(7)	0.00(0)	1.69(27)	0.00(0)	−1.63(24)	0.00(0)	−0.63(23)	0.00(0)	−1.25(24)	0.00(0)	−0.65(30)	0.00(0)	1.38(33)	0.00(0)	−0.54(30)	0.00(0)
$C_{4(5)}$	0.05(7)	−0.74(20)	−0.51(25)	0.46(19)	0.28(24)	−0.74(21)	−1.87(23)	0.76(22)	−0.64(24)	−2.56(35)	−0.59(31)	1.97(32)	1.04(29)	−0.47(26)	−0.81(32)	0.90(30)
$C_{4(7)}$	−0.14(10)	0.85(28)	0.05(28)	−0.70(28)	−0.16(26)	−0.57(26)	−0.04(24)	0.73(26)	−0.81(27)	−0.07(36)	−2.08(31)	0.96(35)	0.68(32)	−1.84(36)	−1.21(33)	−1.96(38)
$C_{5(6)}$	0.00(9)	0.26(28)	−0.16(26)	−0.50(26)	−0.33(28)	0.13(26)	−0.49(26)	−0.10(25)	−0.58(29)	1.54(33)	1.15(38)	−0.59(34)	−0.61(32)	−0.80(34)	0.24(37)	−2.00(37)
$D_{4(7)a}$	−0.05(4)	0.06(33)	−2.08(43)	−0.31(33)	−0.64(44)	0.11(45)	0.29(38)	0.20(44)	−0.45(37)							
$D_{4(7)b}$	−0.02(4)	0.34(28)	0.61(33)	2.10(38)	0.20(32)	0.37(33)	−0.13(39)	0.55(38)	1.28(40)							
$D_{4(7)a}$	0.00(4)	−1.85(35)	0.67(34)	0.08(30)	0.75(41)	−0.42(39)	−0.23(39)	−0.45(33)	−0.53(33)							
$D_{5(6)a}$	−0.01(4)	−1.99(39)	−0.23(29)	0.15(27)	0.69(36)	0.69(38)	−0.31(39)	0.56(31)	−0.61(32)							
$D_{5(6)b}$	0.00(4)	0.20(27)	0.19(28)	1.81(37)	0.17(29)	0.25(32)	−0.36(37)	0.33(35)	0.59(36)							
$D_{5(6)c}$	−0.03(4)	0.34(31)	2.09(39)	−0.63(31)	−0.80(38)	0.21(36)	0.01(38)	−0.18(34)	−0.42(35)							

[a] The form of the expansion was $\rho(r) = \rho_{core}(r) + p_v R_{val}(r) + 4R_{3s}(r)[d_1(r_x + d_2 r_y + d_3 r_z] + R_{3d}(r)[4.717q_1(r_x^2 - r_y^2) + 9.434(q_2 r_x r_y + q_3 r_x r_z + q_4 r_y r_z) + 2.598q_5(3r_z^2 - 1)] + R_{4f}(r)[5.319(\sigma_1(r_x^2 - 3r_y^2)r_x + \sigma_2(3r_x^2 - r_y^2)r_y) + 12.5\sigma_3(r_x^2 - r_y^2)r_z + 25.0\sigma_4 r_x r_y r_z + 4.032(\sigma_5(5r_x^2 - 1)r_x + \sigma_6(5r_y^2 - 1)r_y) + 3.077\sigma_7(5r_z^2 - 3)r_z]$. [b] The refined values of the radial exponents (α) were as follows: radial $N_{(1)}$, 3.32(20); C_2, 3.88(26); $C_{4(5)}$, 2.98(18); $C_{4(7)}$ and $C_{5(6)}$, 3.37(15); D, 2.46(18). [c] The molecular orientation is approximately with the molecular 2-fold along y and C_4–C_5 parallel to x.

density from spherical Hartree–Fock atoms to the bonded arrangement found in **2**. Figure 6a is a cross section of electron density in the molecular plane, and Figure 6b is a cross section 35 pm above the molecular plane. As would be expected, the in-plane deformation density map shows near zero contours at the nuclear positions. The distortion of electron density into the internuclear bonding regions is clearly evident in Figure 6a. The deformation density in the plane of the molecule also shows a very well-defined region of electron density, which corresponds to the σ lone pair of electrons at the carbene center. The deformation density 35 pm above the molecular plane shows very little difference between endo- and exocyclic C–N bonds, which again indicates that there is very little additional density in the endocyclic C–N bonds than could be attributed to π bonding. The endocyclic C–C bond, however, does show a substantial increase in electron density over the exocyclic C–C bonds that is consistent with high double-bond character in the C_4–C_5 bond. Four of the ring atoms (N_1, N_3, C_4, C_5) show near zero contours directly over the nuclear position. By contrast, the carbene center shows a marked deficit in electron density above the plane. This deficit is with respect to the two-thirds of an electron which would occupy the out-of-plane p orbital at the carbene center in the promolecule comprised of spherical Hartree–Fock atoms.

Conclusions

The experimentally determined electron distribution in 1,3,4,5-tetramethylimidazol-2-ylidene-d_{12} (**2**) yields considerable insight into the bonding in this carbene. The in-plane electron distribution in **2** reveals the σ lone pair of electrons that would be expected at a singlet carbene center. Examination of the density above the molecular plane in **2** suggests relatively localized bonding with obvious features corresponding to the C_4–C_5 double bond and nitrogen pπ lone pairs of electrons. The localized π bonding in **2** does not require large contributions from resonance structures **1b** and **1c** to describe the electron distribution. On the contrary, structure **1a** is a wholly adequate depiction of the structure of imidazol-2-ylidenes. The experimentally determined electron distribution in **2** closely matches that calculated by density functional theory and is consistent with previous *ab initio* molecular orbital calculations on imidazol-2-ylidenes.[21] The experimental electron distribution in **2** is very similar to the simple carbene :CF_2.

Because it is evident from our results that π delocalization does not play a dominate role in stabilization of the imidazol-2-ylidenes, the origin of the stability of these carbenes must be elsewhere. The stability question for the imidazol-2-ylidenes is really one of kinetic stability (or reactivity) as opposed to thermodynamic stability.[32] That is to say that the isolation of a stable carbene is dependent upon the ability of the carbene to exist in a deep local minimum on the potential energy surfaces. It is not important what other minima might also exist on the potential surfaces so long as these minima are not kinetically accessible under ambient conditions (that is, there are significant energy barriers to any other potentially lower energy minima). The reactivity of carbenes can be classified into three categories: radical reactivity, electrophilic reactivity, and nucleophilic reactivity.

It is the triplet state of a carbene that is responsible for the radical-like reactivity. Triplet states of the imidazol-2-ylidenes have not been observed. This is borne out by calculations on the imidazol-2-ylidenes that place the triplet state of these carbenes very high in energy (~80 kcal/mol above the singlets).[21] Thus,

(32) We estimate that $\Delta H_{298} = 0.0 \pm 3$ kcal/mol for the dimerization of **2** on the basis of nonlocal density functional theory calculations. $T\Delta S$ for this process at 298 K is −15 kcal/mol on the basis of geometries and frequencies obtained at the MNDO/AM1 level. This corresponds to $\Delta G_{298} = +15$ kcal/mol (endothermic for the dimerization). David A. Dixon, D. A.; Arduengo, A. J., III. To be submitted.

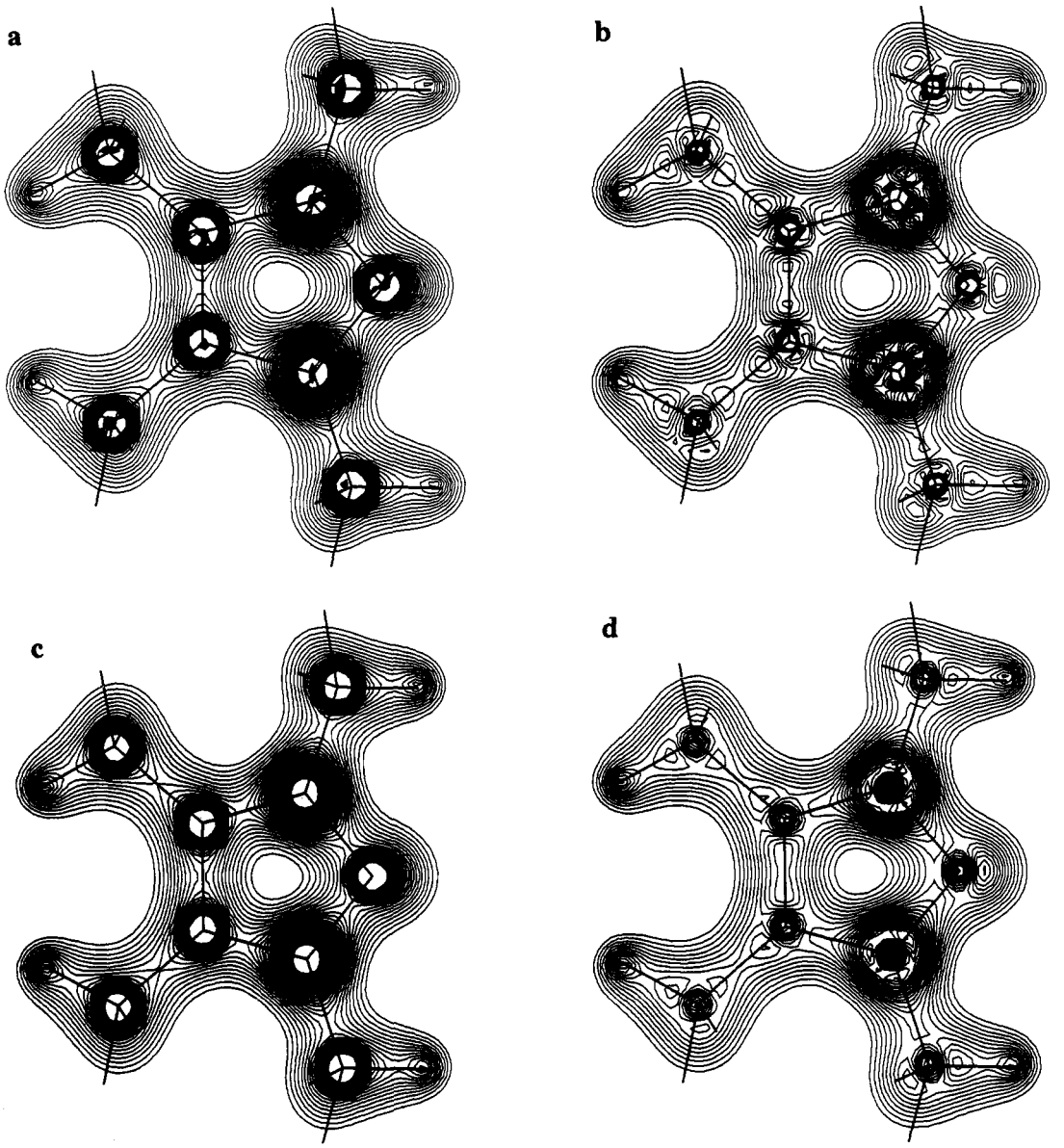

Figure 2. In-plane electron density in **2**. The outermost contour line is 0.65 e Å^{-3} with 0.15 increments between adjacent lines. The total density plots were mapped up to 18.0 e Å^{-3}, and the valence plots were mapped up to 4.33 e Å^{-3}. (a) Experimental total electron density; (b) experimental valence electron density; (c) theoretical (DFT) total electron density; (d) theoretical (DFT) valence electron density.

it is not expected that "triplet reactivity" would be seen for the imidazol-2-ylidenes and therefore could not hinder isolation.

The singlet state of carbenes can give rise to both nucleophilic and electrophilic behavior. Singlet carbenes ($^1A_1$) would be expected to show nucleophilic reactivity by virtue of their σ lone pair electrons and electrophilic reactivity as a result of the vacant p orbital at the carbene center. This dual behavior (ambiphilic reactivity) is evident in what could perhaps be considered the simplest of the carbene reactions, that is, self-reaction or dimerization. This dimerization has been studied computationally for the simplest carbene, CH_2. The calculations show that for singlet carbenes the dimerization should proceed by a non-least-motion pathway involving the nucleophilic perpendicular attack of a carbene lone pair of electrons on the electrophilic vacant out-of-plane p orbital of a second carbene center.[33-37] Indeed a model for the transition state in this dimerization process has been found in the nucleophilic addition of an imidazol-2-ylidene to germanium diiodide.[13] In this way it can be seen that one carbene initially behaves as a nucleophile (the trigonal planar center), whereas the second (the pyramidal center) behaves as an electrophile.

The imidazol-2-ylidenes have been shown to possess considerable nucleophilic reactivity[11-20] but are devoid of electrophilic reactivity. Even adducts of the imidazol-2-ylidenes are reluctant to accept nucleophiles at the 2-position, as demonstrated by stability of the alane (AlH_3) [12] and metal–alkyl (Et_2Mg and Et_2Zn) adducts.[14] The corresponding carbenium (or imidazolium) ion should be particularly susceptible to nucleophilic addition at the 2-position. However, even in this case, nucleophilic addition is difficult and only hydride (H^-) has been found to add easily.[38] The reluctance of an imidazol-2-ylidene to display electrophilic reactivity eliminates a critical component to the dimerization pathway. In other words, with respect to self-reaction (dimerization) the imidazol-2-ylidenes reside in a sufficiently deep minimum that allows their isolation.

(33) Hoffmann, R.; Gleiter, R.; Mallory, F. B. *J. Am. Chem. Soc.* **1970**, *92*, 1460.
(34) Kollmar, H. *Tetrahedron Lett.* **1970**, *38*, 3337.
(35) Sustmann, R.; Binsch, G. *Mol. Phys.* **1971**, *20*, 1.
(36) Fujimoto, H.; Yamabe, S.; Fukui, K. *Bull. Chem. Soc. Jpn.* **1972**, *45*, 1566.
(37) Takabe, T.; Fukutome, H. *Prog. Theor. Phys.* **1976**, *56*, 689.

(38) We have found that 1,3-disubstituted-imidazolium salts can be reduced by $LiAlH_4$ to give the 2*H*-1,3-disubstituted-imidazoles with H_2 at the C_2 position: Arduengo, A. J., III; Dias, H. V. R. Unpublished results.

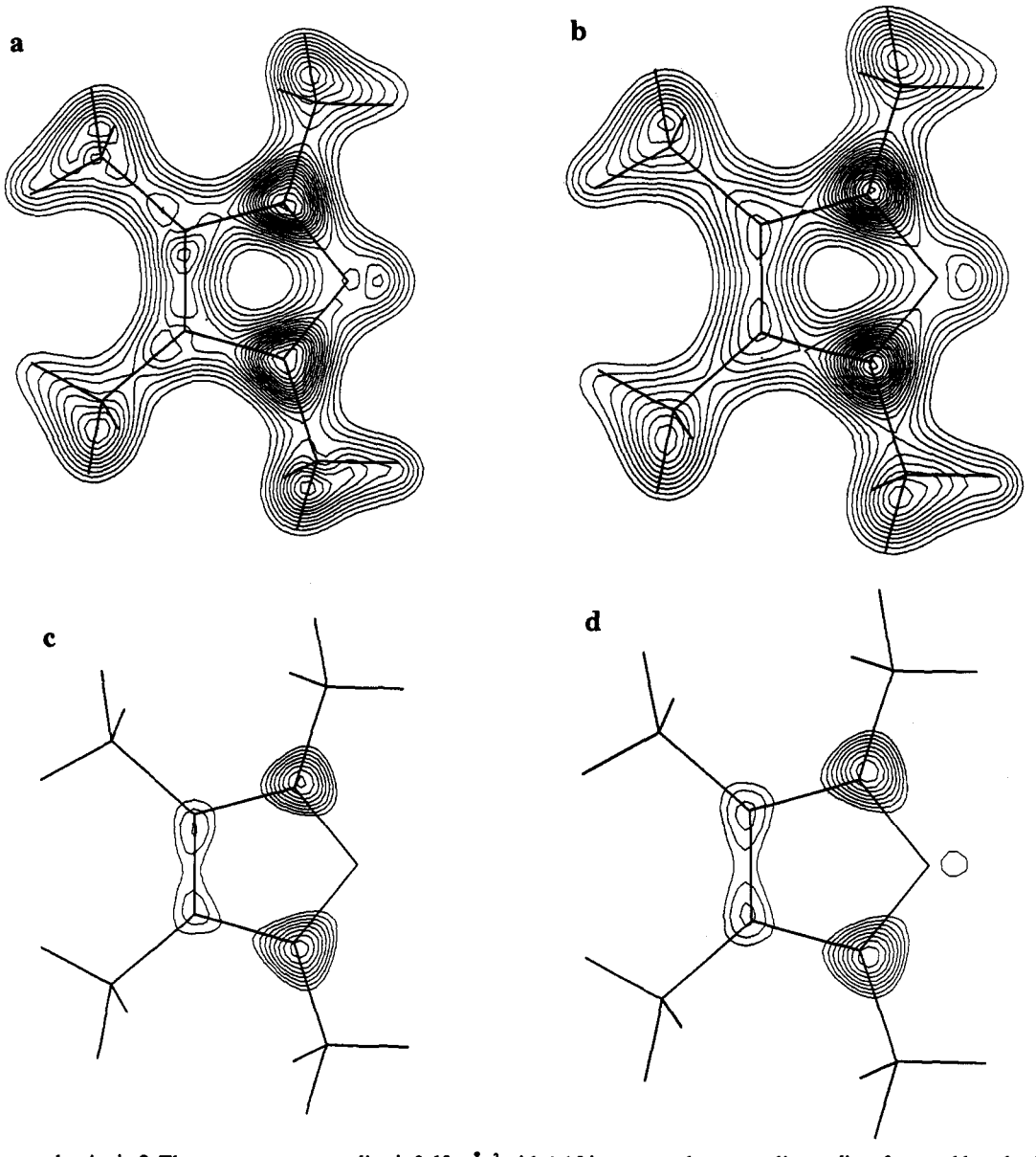

Figure 3. π electron density in **2**. The outermost contour line is 0.65 e Å^{-3} with 0.15 increments between adjacent lines for a and b and 0.05 increments between adjacent lines in c and d. The methyl group contours are omitted from c and d. (a) Experimental valence electron density 35 pm above the molecular plane; (b) theoretical (DFT) valence electron density 35 pm above the molecular plane; (c) experimental valence electron density 70 pm above the molecular plane; (d) theoretical (DFT) valence electron density 70 pm above the molecular plane.

Beyond self-reaction there are a set of very diverse bimolecular reactions of carbenes with other molecules. Among the more common reactions of carbenes are insertion reactions into σ (and π) bonds. These reactions have been widely studied and are well understood.[3,5,6] This C–H insertion reaction (typical of the σ bond insertion reactions) has been demonstrated for both triplet and singlet carbenes. As described above, "triplet reactivity" is not a problem with the imidazol-2-ylidenes. Thus, we again focus on the singlet reactivity. The insertion reactions that have been studied for singlet carbenes suggest that electrophilic reactivity of the carbene is again important.[39,40] The more electrophilic a singlet carbene is, the more rapidly and less selectively it tends to react with C–H bonds.[39] Carbene reactions with π bonds follow a similar trend.[40] The near absence of electrophilic reactivity in the imidazol-2-ylidenes as described above is therefore also responsible for a reluctance of imidazol-2-ylidenes to participate in insertion reactions. This means that media (solvents) such as ethers and hydrocarbons can be used as solvents for the imidazol-2-ylidenes without fear of reactions with the solvent. Compare this situation to that of the more electrophilic carbenes that can only be matrix "isolated" in frozen noble gas or fluorocarbon media. The ability to use the more common organic solvents greatly facilitates the isolation of the imidazol-2-ylidenes.

The experimentally determined electron distribution in **2** provides an explanation of the lack of electrophilic reactivity. The minimal electrophilicity found for the imidazol-2-ylidenes is the likely result of electron repulsion. The high electron density (lone pair) found at the carbene center of **2** would provide considerable electron repulsion to a nucleophile approaching from above or below the molecular plane at C_2, as usual for nucleophilic addition to any singlet carbene. However, in the case of the imidazol-2-ylidenes this electron repulsion is augmented with the high $p\pi$ lone pair density found on the nitrogen centers adjacent to C_2, thus causing considerable additional electron repulsion of any incoming nucleophile. The $C_4{=}C_5$ double bond further enhances this effect by providing additional π electron density to the more electronegative nitrogens. The imidazolin-2-ylidenes (saturated in the 4- and 5-positions) studied by Wanzlick have never been isolated, which supports the view that the $C_4{=}C_5$ double bond is critical in amassing the necessary

(39) See ref 5, Chapter 7, p 209.
(40) See ref 3, Chapter 2, p 153.

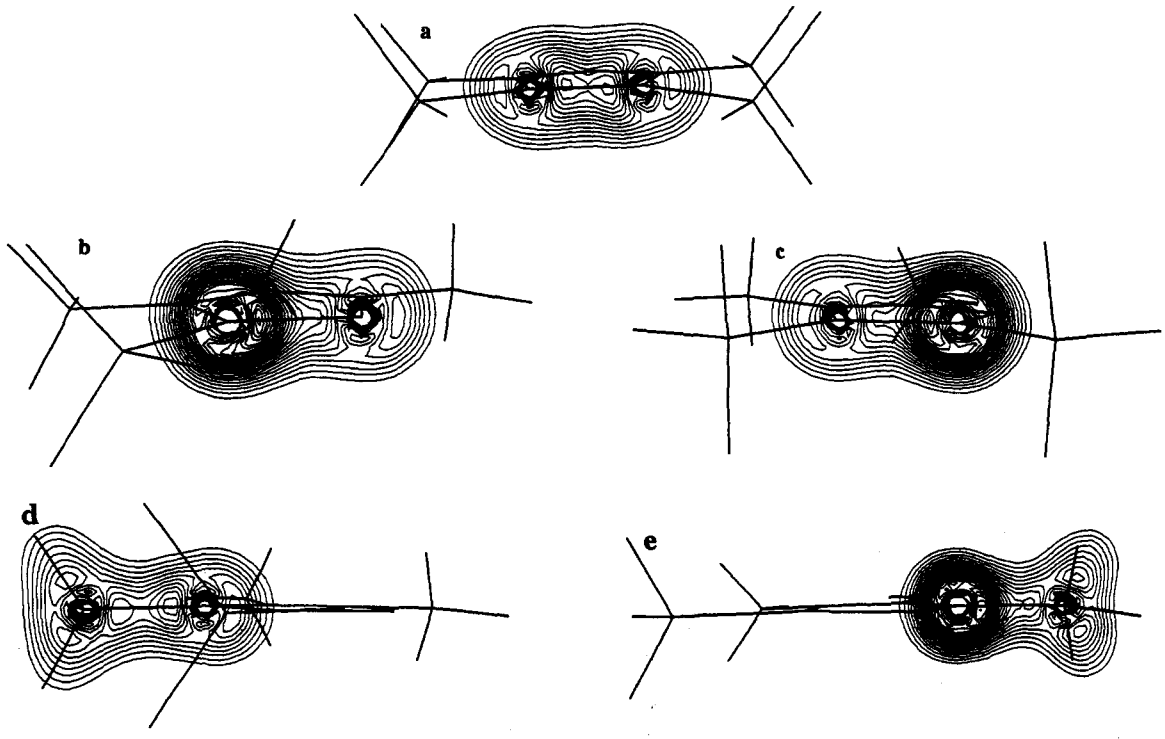

Figure 4. Experimental out-of-plane electron density perpendicular to the molecular plane in **2**. The outermost contour line is 0.65 e Å^{-3} with 0.15 increments between adjacent lines. (a) C_4-C_5 density; (b) C_2-$N_{3(1)}$ density; (c) $C_{4(5)}$-$N_{3(1)}$ density; (d) exocyclic C–C bond density; (e) exocyclic C–N bond density.

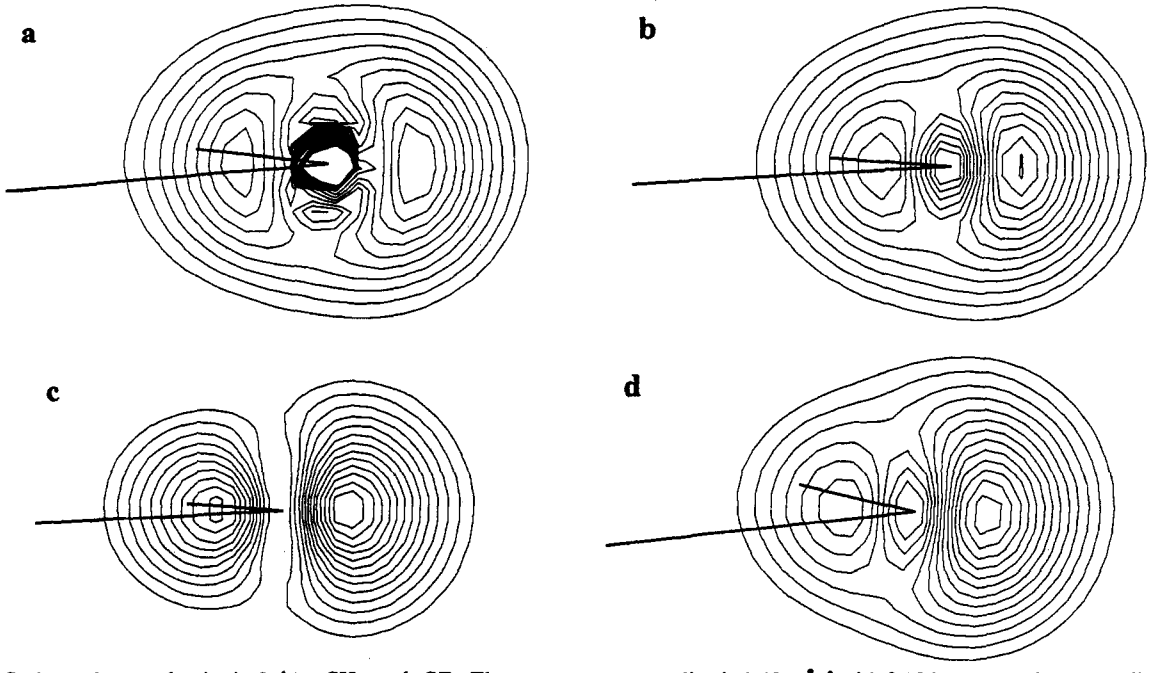

Figure 5. Carbene electron density in **2**, $^1A_1$:CH_2, and :CF_2. The outermost contour line is 0.65 e Å^{-3} with 0.15 increments between adjacent lines. (a) Experimental valence electron density in **2**; (b) theoretical (DFT) valence electron density in **2**; (c) theoretical (DFT) valence electron density in $^1A_1$:CH_2; (d) theoretical (DFT) valence electron density in :CF_2.

electron repulsion to deprive the carbene of electrophilic reactivity.[41] The experimental and theoretical electron densities described herein for **2** provide proof of the accumulated electron density that surrounds the carbene center protecting the imidazol-2-ylidenes from nucleophilic additions and thus kinetically stabilizes the molecules.

The structural and electronic features that have led to the moderation of the electrophilic reactivity that can hinder the isolation of carbenes have left the imidazol-2-ylidenes with a high degree of nucleophilic reactivity. This nucleophilic reactivity is the object of ongoing studies that are demonstrating the variety of reactivity that is typical of nucleophilic carbenes.[11-20]

Experimental Section

Reactions and manipulations were carried out under an atmosphere of dry nitrogen, either in a Vacuum Atmospheres drybox or using standard Schlenk techniques. Solvents were dried (using standard procedures),[42] distilled, and deoxygenated prior to use, unless otherwise indicated.

(41) Lachmann, B.; Steinmaus, H.; Wanzlick, H.-W. *Tetrahedron* **1971**, *27*, 4085.

(42) Perrin, D. D.; Armarego, W. L. F.; Perrin, D. R. *Purification of Laboratory Chemicals*; Pergamon: New York, 1985.

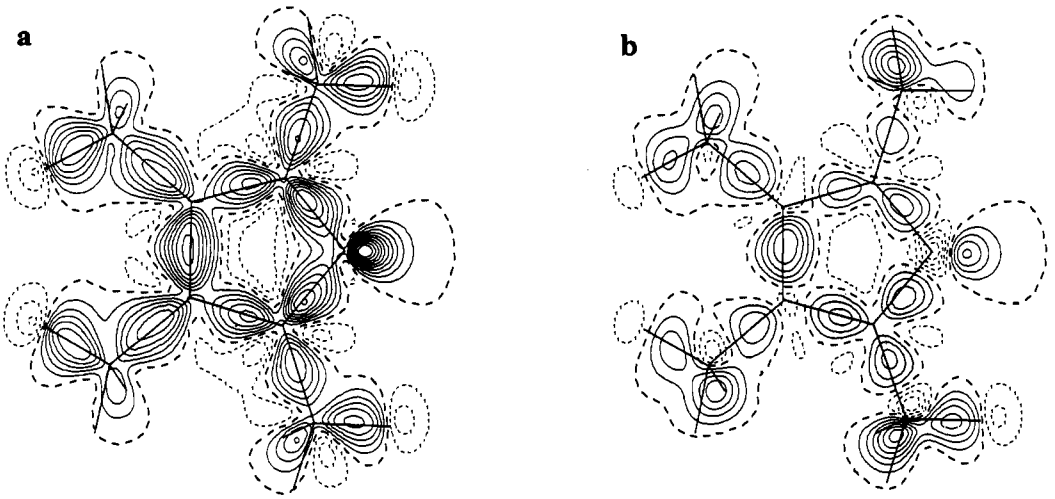

Figure 6. Deformation density contours in **2** (intervals of 0.1 e Å^{-3}). The promolecule for these plots was comprised of spherical atoms. Solid contours represent a surplus of electron density relative to the promolecule, dashed lines represent a deficit of electron density, and the zero contour is the heavy dashed line. (a) The deformation density in the plane of the molecule; (b) the deformation density 35 pm above the molecular plane.

Glassware was oven-dried at 160 °C overnight. The ^{1}H (300.75 MHz), ^{2}H (46.133 MHz), and ^{13}C (75.629 MHz) NMR spectra were recorded on a GE Omega 300WB spectrometer. The NMR reference is $(CH_3)_4Si$ (^{1}H, ^{2}H, ^{13}C). Melting points were obtained on a Thomas–Hoover capillary apparatus and were not corrected. Elemental analyses were performed by Oneida Research Services, Whitesboro, NY.

Formaldehyde in D_2O. Paraformaldehyde (12 g) and D_2O (22 g, purged with N_2 for 10 min), CD_3OD (6 g), and a small stir bar were placed in a heavy-walled pressure tube (16 mm × 9 inches) and sealed (under slightly reduced pressure). The tube was heated at 98 °C for 3 days. Paraformaldehyde slowly dissolved and gave a clear solution. The tube was cooled at 0 °C and opened. The resulting solution (30% w/w CH_2O) was stored under nitrogen at room temperature until needed.

Methylamine-d_5 in D_2O. A 400-mL Parr shaker vessel was charged with 300 mL of D_2O, 2.0 g of 5% Pd/charcoal, and 55 g of CD_3NO_2 (Aldrich, 99 atom % D). The vessel was connected to the shaker apparatus and purged with N_2 by alternate evacuation to 200 mmHg and charging to 12 psig (10 cycles). The vessel was evacuated to 200 mmHg, charged with 15 psig D_2 (Alfa Products, 99.995%), and evacuated back to 200 mmHg *without shaking*. Deuterium was added to a pressure of 70 psig, and shaking was started. The vessel was heated to 60 °C with an air gun. Deuterium was absorbed at the rate of about 267 mL/min initially. After 2 h the rate of D_2 uptake was about 33 mL/min, and 37% of the theoretical D_2 had been adsorbed. The pressure was increased to 80 psig. After 5 h the uptake of deuterium was extremely slow. The vessel was brought to atmospheric pressure and purged with N_2. The Parr vessel was opened, 2 g of Pearlman's catalyst[43] (Aldrich, 20% Pd, washed with 75 mL of D_2O) was added in a single portion, and the reduction was continued as before. The uptake of D_2 was about 133 mL/min. After shaking overnight, 70% of the theoretical D_2 was adsorbed. The vessel was brought to atmospheric pressure and purged with N_2. The Parr vessel was opened, 2 g of 5% Pd/charcoal was added in a single portion, and the reduction was continued as before for an additional 6 h. The pressure in the Parr vessel was released and the D_2 purged from the vessel with N_2 as before (1 cycle). The solution was filtered through Celite under N_2 pressure. Sodium chloride (120 g) was added to the filtrate. The methylamine-d_5 and some D_2O were distilled from the salted filtrate at atmospheric pressure to give ~78 mL of distillate, which was collected at −78 °C. The concentration of the aqueous amine was determined to be 4.944 M by titration of a 0.5-mL aliquot of the solution dissolved in 10 mL of H_2O with 0.098 M HCl (methyl red indicator). Isolated yield of amine was 45% of theory.

2,3-Butanedione-d_6. Butane-2,3-dione was H/D exchanged with D_2O and D_2SO_4 catalyst for seven cycles. For each successive cycle the volumes of D_2O and D_2SO_4 were adjusted to reflect the amount of butanedione used in that cycle. For the initial cycle, 2,3-butanedione (100 g), D_2O (200 mL), and D_2SO_4 (2 mL) were heated at 95 °C for 12 h. The 2,3-butanedione was isolated by distillation at atmospheric pressure (78–80 °C) and separation from the D_2O, which codistilled. The 2,3-butanedione thus isolated was used without further purification for the next cycle. After the final cycle and isolation the 2,3-butanedione-d_6 was dried over anhydrous magnesium sulfate. The yield after seven cycles was 39.6 g of 99.2 atom % D (from EI-MS data) 2,3-butanedione-d_6.

Methyl Chloride-d_3. Perdeuteriomethyl chloride was prepared by a modification of the procedure reported by Weiss *et al.*[44] Ferrous sulfate scrubbers were added to remove chlorine from the product stream.

Methanol-d_4 (44.7 g) (Aldrich, 99.8 atom % D) was added dropwise at room temperature to $POCl_3$ (250 mL) in a three-necked 500-mL flask equipped with a reflux condenser and magnetic stirrer. Deuterium chloride was generated during the addition. After the addition was complete the mixture was stirred for 30 min and transferred to an addition funnel under a blanket of dry N_2. This addition funnel was connected to a 1-L, three-necked flask containing PCl_5 (340 g) and equipped with a reflux condenser, a N_2 inlet, and a stirrer. The top of the reflux condenser was connected to a series of traps. The first trap was empty and was followed by a H_2O trap maintained at 0 °C, two saturated aqueous $FeSO_4$ traps, a concentrated H_2SO_4 trap, another empty trap, a trap to collect CD_3Cl at −78 °C, and an oil bubbler. This setup was purged with N_2 for 15 min, and then the $POCl_3$/deuteriomethanol mixture was added at room temperature over a period of 15–30 min. Throughout the reaction a small N_2 stream was maintained. After the addition was complete, the mixture was refluxed for 2 h (~110 °C). The mixture was allowed to cool to room temperature, and N_2 was bubbled through the mixture for 15 min; the resulting colorless CD_3Cl-containing trap was removed from the system, and CD_3Cl was transferred to a glass bomb containing 3-Å molecular sieves. The yield was 27 g (41%) >99.6 atom % D.

1-propanol-*O*-*d* Propanol-*O*-*d* was prepared by reacting 1-propanol with sodium hydride in tetrahydrofuran and quenching with D_2O. Careful distillation is required to separate the THF and propanol-*O*-*d* product.

1,4,5-Trimethylimidazole-d_9. The trimethylimidazole was synthesized by a modification of the method of Graf and Hupfer.[45]

Hexadeuteriobiacetyl ($CD_3COCOCD_3$, 22.74 g, 0.247 mol), CH_2O (24.7 g of a 30% solution in D_2O) and 1-propanol-*O*-*d* (10 mL) were mixed and placed in an addition funnel. Ammonia-d_3, 26% solution in D_2O (MSD, 99 atom % D) (19.0 g), and CD_3ND_2 (50.0 mL of 4.94 M solution in D_2O) were combined in a second addition funnel. The contents of the two funnels were added simultaneously over a 10-min period to 1-propanol-*O*-*d* (20 mL) at 70 °C. This mixture was heated for 30 min after the addition was complete. The volatiles were removed on a Rotovap, and the product was vacuum distilled at 65 °C (~0.3 mmHg) to give 12.66 g (43%) of 1,4,5-trimethylimidazole-d_9. NMR: ^{2}H (C_6H_6) δ 1.62 (s, CCD_3, 3 D), 2.28 (s, CCD_3, 3 D), 2.48 (s, NCD_3, 3 D), 7.06 (s, N_2CD, 0.6 D); ^{1}H (C_6D_6) δ 1.62 (m, $CCHD_2$, 0.17 H), 2.22 (m, $CCHD_2$, 0.17 H), 2.58 (m, $NCHD_2$, 0.09 H), 7.04 (s, N_2CH, 1 H).

1,3,4,5-Tetramethylimidazolium-d_{12} Chloride. Tetrahydrofuran (35 mL) and 1,4,5-trimethylimidazole-d_9 (15 g, 125 mmol) were placed in a glass pressure tube (110-mL capacity) and degassed with one freeze–

(43) Fieser, L. F.; Fieser, M. *Reagents for Organic Synthesis*; John Wiley and Sons, Inc.: New York, 1967; Vol. 1.

(44) Weiss, E.; Lambertsen, T.; Schubert, B.; Cockcroft, J. K. *J. Organomet. Chem.* **1988**, *358*, 1.

(45) Graf, F.; Hupfer, L. U.S. Patent 4450277, 1984.

thaw cycle. On a vacuum line, methyl chloride-d_3 (13 g) was condensed into the tube with cooling from liquid nitrogen, and the tube was sealed. This mixture was allowed to warm to room temperature, mixed well, and kept undisturbed for 3 days. Colorless crystals were formed in the tube. The crystalline 1,3,4,5-tetramethylimidazolium-d_{12} chloride was collected by filtration, rinsed with 4 × 30 mL of diethyl ether, and dried under vacuum. Yield: 16.62 g (76.6%). Mp: 230–231 °C. NMR: ^{2}H (DMSO) δ 2.20 (s, CCD_3, 6 D), 3.72 (s, NCD_3, 6 D), 9.28 (s, N_2CD, 0.6 D), ^{1}H (DMSO-d_6) δ 2.23 (m, $CCHD_2$, 0.18 H), 3.75 (m, $NCHD_2$, 0.07 H), 9.27 (s, N_2CH, 1 H); ^{13}C (DMSO)$\{^2H, ^1H\}$ δ 7.25 (s, CCD_3), 32.70 (s, NCD_3), 126.83 (s, NCC) 135.04 (s, NCN). Melting point and NMR spectra confirm the identity of the product by comparison with an authentic sample of the all-protio analog.[8]

A small amount (1.93 g) of 1,4,5-trimethylimidazole-d_9 was recovered from the THF filtrate and ether washes.

1,3,4,5-Tetramethylimidazol-2-ylidene-d_{12}. The procedure used for the protio analog was followed.[8] Oil-free sodium hydride (0.950 g, 39 mmol) and 1,3,4,5-tetramethylimidazolium-d_{12} chloride (6.0 g, 34 mmol) were mixed in THF (20 mL) and stirred for 5 min. To this suspension was added potassium *tert*-butoxide (0.200 g, 1.78 mmol) in THF (5 mL) at room temperature and stirred until no H_2 evolution was observed (~3.5 h, H_2 evolution peaked between 45–60 min). The solution became light yellow. The mixture was filtered over Celite, the residue was rinsed with THF (3 × 15 mL portions), and the volatiles were removed from the combined filtrate under vacuum. The crude carbene (4.4 g, 95%) was isolated as pale green crystals. This material could be recrystallized from warm hexane/toluene to give nearly colorless 1,3,4,5-tetramethylimidazol-2-ylidene-d_{12}, mp 109–111 °C. A 0.25-g sample of the carbene was sublimed under vacuum at 50 °C (0.1 mmHg). The carbene sublimed easily and quickly to afford colorless crystals (0.197 g), mp 108 °C. NMR: ^{2}H (THF) δ 2.01 (s, CCD_3, 6 D), 3.50 (s, NCD_3, 6 D), ^{13}C (THF)$\{^2H\}$ δ 7.73 (s, CCD_3), 34.06 (s, NCD_3), 122.47 (s, NCC), 212.47 (s, NCN). NMR spectra (^{2}H, ^{13}C) confirm the identity of the product, in accord with the literature report.[8]

X-ray Data Collection and Structure Refinement. A crystal of dimensions 0.20 × 0.20 × 0.25 mm was mounted on a Syntex R3 diffractometer equipped with graphite-monochromatized Mo Kα radiation (λ = 71.069 pm) and with a low-temperature apparatus, which kept the crystal cooled to 173 K. The unit cell of **2** was found to be very similar to its protio relative.[8] The lattice parameters were refined from the computer-centered positions of 48 reflections. Four octants of data were collected to yield an R_{merge} of 0.019 (ω-scans with variable scan speeds of 2.9–11.7 deg/min^{-1}; $4° < 2\theta < 70°$; three standard reflections showed a 2.0% fluctuation in intensity during the data collection; an azimuthal scan varied by 2.2%). The atomic coordinates for the protonated form, being isostructural, were used to begin the refinement; all of the atoms were eventually refined with anisotropic thermal parameters. Tables 1 and 2 list the crystallographic details.

The refinement and analysis of the structure were carried out using a package of local programs.[46] The atomic scattering factors were taken from the tabulations of Cromer and Waber;[47] anomalous dispersion corrections were by Cromer and Ibers.[48] In the least-squares refinement, the function minimized was $\Sigma w(|F_o| - |F_c|)^2$ with the weights, w, assigned as $[\sigma^2(I) + 0.0009I^2]^{-1/2}$.

Neutron Data Collection and Structure Refinement. The carbene crystals were synthesized as described above. The crystal selected for the neutron diffraction study exhibited forms {110,001} and had dimensions 3.3 × 3.3 × 2.0 mm, 21.8 mm^3. The sample was covered in a protective film of halocarbon grease, mounted along its c-axis on an aluminum pin, and sealed inside an aluminum canister under a helium atmosphere. The data were collected on the four-circle diffractometer at port H6S of the Brookhaven High Flux Beam Reactor. The neutron beam, monochromated by Ge(220) planes in transmission geometry, had a wavelength of 115.84(1) pm, as calibrated against a KBr crystal (a_0 = 660.00 pm at 295 K). During the 3 weeks of measurements, the crystal temperature was held at 80 ± 0.1 and 173 ± 0.1 K inside a two-stage DISPLEX helium cryostat. The lattice parameters at each temperature were determined by a least-squares fit of $\sin^2\theta$ values for 32 reflections within the range $45° < 2\theta < 55°$. Intensity data of two quadrants [$\pm h, \pm k, l$; $|h| \le 8, |k| < 5, 1 \le 8$; $\sin\theta/\lambda < 0.43$ Å^{-1}] and [$\pm h, \pm k, \bar{1}$, ; $|h| \le 13, |k| \le 9, |l| \le 14$; $0.43 < \sin\theta/\lambda < 0.70$Å^{-1}] were measured using scan widths $\Delta 2\theta = 3.2°$ for $\sin\theta/\lambda \le 0.43$ Å^{-1} and $\Delta 2\theta = (1.60 + 3.15 \tan\theta)°$ for $\sin\theta/\lambda > 0.43$ Å^{-1}. The intensities of two reflections [$\bar{4}$ 4 4; 7 1 1] monitored at regular intervals showed no systematic variations. Integrated intensities I_0 and variances $\sigma^2(I_0)$ were derived from the scan profiles as described previously.[49] Absorption corrections[50,51] were applied using μ_n = 0.013 cm^{-1}, based on μ/ρ values given in *International Tables for X-ray Crystallography*.[52] Minimum and maximum transmission factors were 0.996 and 0.998. Averaging the 80 K F_o^2 values of 810 symmetry-related pairs of reflections resulted in an internal agreement factor of 0.019. These averaged reflections were grouped with an additional 68 reflections, which were measured only once and yielded 878 independent observations, of which only one had a value more negative than $1\sigma(F_o^2)$. Averaging the 173 K F_o^2 values of 814 symmetry-related pairs of reflections resulted in an internal agreement factor of 0.022. These averaged reflections were grouped with an additional 84 reflections, which were measured only once and yielded 898 independent observations, of which 17 were negative, only two of these by more than $1\sigma(F^2_o)$.

For the refinement model, starting nuclear parameters of all atoms were taken from the X-ray analysis (see above). Coherent neutron-scattering lengths (fm) for D (6.674), C (6.648), and N (9.37) were taken from the tabulation of Koester.[53] Refinement of the completed model of 11 independent atoms was carried out by full-matrix least-squares methods using the program UPALS.[54] The quantity $\sum w|F_o^2 - F_c^2|^2$ was minimized with weights $w = [\sigma^2(F_o^2) + (0.01F_o^2)^2]^{-1}$, summing over the independent observations. The variable parameters were one scale factor, coordinates and anisotropic β_{ij} for all atoms, except for C_2, where x, z, β_{12}, and β_{23} were not refined due to symmetry constraints, and the anisotropic extinction parameters g_{ij} for a type I crystal.[55,56] The scattering factors of the deuteriums were also refined at one point and later fixed at average values of 0.666 (99.9% D) and 0.649 (98.3% D) for deuteriums on $C_{6(7)}$ and $C_{9(8)}$, respectively. The refinement converged $(\Delta p_i/\sigma(p_i) < 0.001)$ with fit indices $R(F_o^2)$ = 0.030; $wR(F_o^2)$ = 0.061; $wR(F_o)$ = 0.058; and S = 4.09, for the 80 K data, and $R(F_o^2)$ = 0.035; $wR(F_o^2)$ = 0.053; $wR(F_o)$ = 0.038; and S = 2.88, for the 173 K data, based on all reflections, except 202. The formulas used here are $R(F_o^n) = \sum\Delta/\sum F_o^n$; $wR(F_o^n) = [\sum w\Delta^2/\sum(wF_o^n)^2]^{1/2}$; $S = [\sum w\Delta^2/(m-p)]^{1/2}$; where $\Delta = |F_o^n| m$ and p are the numbers of observations and parameters, respectively, and n is 1 for refinement based on F_o and 2 for refinement based on F_o^2. In the final ΔF map, the largest $|\Delta\rho|$ errors were <5% of the peak maximum for carbon in the ρ_o map.

There are significant extinction corrections. At 80 K there are 19 reflections which have an extinction correction larger than 1.3, the largest correction being 1.72 for reflection $1\bar{3}2$; at 173 K there are 12 reflections which have an extinction correction larger than 1.3, the largest being 1.61 for the same reflection.

Electron Density Distribution at 173 K. The electron density distribution in the crystal structure at 173 K was determined by least-squares refinement based on the rigid pseudoatom model of Stewart.[57] The pseudoatoms were assumed to be isolated neutral Hartree–Fock atoms. Charge deformation terms were introduced. Each deformation term was assigned a Slater-type radial function with a variable value for the radial exponent (α) for each atom. Angular functions were obtained from a complete multipole expansion about each pseudoatom nucleus up to the octapole level (quadrupole for H atoms). For details of the X-ray

(46) Calabrese, J. C. Central Research and Development, E. I. du Pont de Nemours and Co., P. O. Box 80228, Wilmington, DE 19880-0228, 1991.

(47) Cromer, D. T.; Waber, J. T. International Tables for X-ray Crystallography (Atom Scattering Factors). In *International Tables for X-ray Crystallography*; Ibers, J. A., Hamilton, W. C., Eds.; Kynoch Press (present distributor D. Reidel, Dordrecht): Birmingham, 1974; Vol. IV, p 71.

(48) Cromer, D. T.; Ibers, J. A. International Tables for X-ray Crystallography (Anomalous dispersion). In *International Tables for X-ray Crystallography*; Ibers, J. A., Hamilton, W. C., Eds.; Kynoch Press (present distributor D. Reidel, Dordrecht): Birmingham, 1974; Vol. IV, p 148.

(49) McMullan, R. K.; Epstein, J.; Ruble, J. R.; Craven, B. M. *Acta Crystallogr.* **1979**, *B35*, 688.

(50) de Meulenaer, J.; Tompa, H. *Acta Crystallogr.* **1965**, *19*, 1014.

(51) Templeton, L. K.; Templeton, D. H. *Abstracts of Papers*, American Crystallography Association Meeting, Storrs, CT, 1973; p 143.

(52) Lipson, H.; Bond, W. L.; Decker, B. F.; Hargreaves, A.; Kraut, J.; Nordman, C. E.; Sullivan, R. A. L. International Tables for X-ray Crystallography (Absorption Corrections). In *International Tables for X-ray Crystallography*; Kasper, J. S., Lonsdale, K., Eds.; Kynoch Press (present distributor D. Reidel, Dordrecht): Birmingham, 1972; Vol. II, p 291.

(53) Koester, L. Neutron Physics. In *Springer Travts in Modern Physics*; Hohler, G., Ed.; Springer: Berlin, 1977; p 36.

(54) Lundgren, J. *UPALS; A Full-matrix Least-squares Refinement Program.* Report UUICB13-4-05; Institute of Chemistry, University of Uppsala: Sweden.

(55) Becker, P. J.; Coppens, P. *Acta Crystallogr.* **1974**, *A30*, 129.

(56) Thornley, F. R.; Nelmes, R. J. *Acta Crystallogr.* **1974**, *A30*, 748.

(57) Stewart, R. F. *Acta Crystallogr.* **1976**, *A32*, 565.

scattering factors for the deformation terms, see Epstein, Ruble, and Craven.[58]

The multipole refinements were done with the program POP.[59] Atomic scattering factors were those as calculated by Cromer and Waber for C and N.[47] For H spherical bonded atom scattering factors were assumed.[60] Anomalous dispersion corrections were included.[48]

The pseudoatom refinement was based on F and involved 1513 reflections, 110 being omitted. The positional and displacement parameters from the neutron refinement were used (*vide supra*). The variables consisted of the scale factor, the radial exponents, the electron population parameters (for C_2 as far as allowed by symmetry), and an isotropic extinction parameter for a type I crystal.[55] The isotropic extinction parameter was omitted after it failed to assume a significantly nonzero value, giving a total of 132 variables. The quantity $\sum w|F_o^2 - F_c^2|$ was minimized with weight $w = 1/\sigma^2$. The variance was taken to be $\sigma^2 = \sigma_{cs}^2 + (0.01F_o)^2$. The refinement resulted in $R(F_o^2) = 0.066$; $wR(F_o^2) = 0.037$; and $S = 0.86$. The residual map shows that there are no significant features remaining. The final values for positional and anisotropic displacement parameters from the neutron analysis are listed in Tables 2-4. The electron population parameters are listed in Table 5.

The sum of the monopole population parameters must be 0 for the unit cell to be neutral. The sum observed for the pseudoatoms for one molecule was −0.30(12), which is not significantly different from 0. Since there are 68 electrons in one molecule, the model accounts for 99.6% of the total. The electron population parameters have been scaled by 1.004 so as to give a neutral unit cell.

Theoretical Methods. The density functional theory[61-65] calculations were done with the program DGauss,[66-69] which employs Gaussian orbitals on a Cray YMP computer. Calculations were done with all electrons and with pseudopotentials for carbon and nitrogen. The all-electron basis set[70] is a polarized valence triple ζ set (TZVP) for carbon and nitrogen with the form (7111/4111/1) and an [8/4/4] fitting basis set, whereas for hydrogen a polarized double ζ basis set was used with the form (41/1) and a fitting basis set of the form [4/1]. Norm-conserving pseudopotentials[30] were generated for carbon and nitrogen following the work of Troullier and Martins.[31] The valence basis sets are [3/2/1] with a fitting basis set of [5/4] for carbon and [6/4] for nitrogen. The calculations were done at the self-consistent gradient corrected (nonlocal) level with the nonlocal exchange potential of Becke[26-28] together with the nonlocal correlation functional of Perdew (BP).[29] The local potential fit of Vosko, Wilk, and Nusair was used.[71] The calculations were done at the experimental geometry obtained from the neutron diffraction experiments. In order to obtain a good resolution in the mesh, the electron density was calculated at ~10-pm intervals. The experimental electron densities calculated as described above were read into the UniChem interface by using the facilities provided in the Attachers Toolkit. The geometries of ^{1}:CF_2 and ^{1}:CH_2 were optimized at the TZVP/BP level (r_{CF} = 132.9 pm, θ_{FCF} = 104.3°, r_{CH} = 112.6 pm, θ_{HCH} = 100.4°).

Acknowledgment is made for the excellent technical assistance of H. A. Craig (DuPont), L. F. Lardear (DuPont), and T. J. O'Loughlin (Brookhaven). The assistance of Scott C. Walker (DuPont) for the production of Figures 2–6 is greatly appreciated. The import of the experimental electron density into the UniChem interface for plotting and comparison with the theoretical densities was made possible by Patrick J. Capobianco (Cray Research). Frederic Davidson (DuPont) kindly provided the ^{1}H, ^{2}H, and ^{13}C NMR spectra. The neutron diffraction study and structure refinement were carried out at Brookhaven National Laboratory under contract DE-AC02-76CH00016 with the U.S. Department of Energy and supported by its Office of Basic Energy Sciences, Division of Chemical Sciences.

Supplementary Material Available: Lists of structure factors for the three diffraction studies (14 pages). This material is contained in many libraries on microfiche, immediately follows this article in the microfilm version of the journal, and can be ordered from the ACS; see any current masthead page for ordering information.

(58) Epstein, J.; Ruble, J. R.; Craven, B. M. *Acta Crystallogr.* **1982**, *B38*, 140.
(59) Craven, B. M.; Weber, H. P.; He, X. M. *The POP Least-Squares Refinement Procedure.* Technical Report; University of Pittsburgh: Pittsburgh, PA, 1987.
(60) Stewart, R. F.; Davidson, E. R.; Simpson, W. T. *J. Chem. Phys.* **1965**, *42*, 3175.
(61) Parr, R. G.; Yang, W. *Density Functional Theory of Atoms and Molecules*; Oxford University Press: New York, 1989.
(62) Salahub, D. R. *Ab Initio Methods in Quantum Methods in Quantum Chemistry-II*; Lawlwy, K. P., Ed.; J. Wiley & Sons: New York, 1987; p 447.
(63) Wimmer, E.; Freeman, A. J.; Fu, C.-L.; Cao, P.-L.; Chou, S.-H.; Delley, B. *Supercomputer Research in Chemistry and Chemical Engineering*; ACS Symposium Series # 353; American Chemical Society: Washington, DC, 1987.
(64) Jones, R. O.; Gunnarsson, O. *Rev. Mod. Phys.* **1989**, *61*, 689.
(65) Zeigler, T. *Chem. Rev.* **1991**, *91*, 651.
(66) Andzelm, J. W.; Wimmer, E.; Salahub, D. R. *The Challenge of d and f Electrons: Theory and Computation*; ACS Symposium Series # 394; American Chemical Society: Washington, DC, 1989.
(67) Andzelm, J. W. *Density Functional Methods in Chemistry*; Springer-Verlag: New York, 1991.
(68) Andzelm, J. W.; Wimmer, E. *J. Chem. Phys.* **1992**, *96*, 1280.
(69) DGauss is a density functional program available via the Cray Unichem Project
(70) Godbout, N.; Salahub, D. R.; Andzelm, J. W.; Wimmer, E. *Can. J. Chem.* **1992**, *70*, 560.
(71) Vosko, S. J.; Wilk, L.; Nusair, M. *Can. J. Phys.* **1980**, *58*, 1200.